Journal of Physics: Conference Series **2494** (2023) 012001 doi:10.1088/1742-6596/2494/1/012001

Multi-qubit BEC trap for atomic boson sampling

William Shannon, Vitaly Kocharovsky

Department of Physics and Astronomy and Institute for Quantum Science and Engineering, Texas A&M University, College Station, TX 77843-4242, USA

E-mail: wshannon@tamu.edu, vkochar@physics.tamu.edu

Abstract. We suggest a new platform for examination of quantum statistical phenomena in many-body interacting systems – a multi-qubit Bose-Einstein-condensate (BEC) trap. Ideally, it is suitable for demonstrating manifestations of quantum supremacy of such systems through atomic boson sampling of excited-state occupations. This is wholly different than the linear-interferometer platform which uses Gaussian boson sampling of non-interacting non-equilibrium photons rather than interacting atoms in equilibrium. We present a basic model of the multi-qubit BEC trap and illustrate its essential properties by means of numerical simulations.

1. Introduction

Much of the current work on quantum computing is dedicated toward demonstration of its quantum supremacy over classical computing. Various techniques have been discussed and employed to try to achieve this goal which has so far been elusive [1]. Here we present a new platform suitable for such research; a multi-qubit BEC trap [2]. It stems from the fact of computational ♯P-hardness of atomic boson sampling of excited-atom numbers in a Bose-Einstein-condensed interacting equilibrium gas proven in [3]. This comes as an alternative to the well-known optical interferometer platform which makes use of non-interacting photons, supplied in squeezed states by external sources, rather than massive atoms in equilibrium [4, 5, 6, 7].

1.1. Computational ♯P-hardness and quantum supremacy of photonic boson sampling in a linear interferometer

Both boson sampling problems, photonic in the linear interferometer and atomic in the BEC trap, are ♯P-hard for computing. This stems from the fact that both derive their complexity from the hafnian (or indeed the permanent) of some $n\times n$ matrix composed from a correlation matrix G of the creation and annihilation operators of associated bosons [3, 8]. The hafnian and permanent constitute a universal tool for studying nature's complexities [9] and their computation is a ♯P-hard problem [10], requiring $\sim n^3 2^{n/2}$ and $\sim n^2 2^n$ operations, respectively.

Until now the most promising was Gaussian boson sampling in a linear interferometer [5, 6, 7]. Squeezed photons enter an optical network which scatters them as they pass through different channels. Ideally this process is described by a unitary U which encodes all of the information about the system. The issue then is to produce a sufficiently varied sample of outputs.

There are, however, some limiting factors that have halted proving quantum supremacy with such a system. The most serious one is photon loss that grows exponentially with the size of the system. Another complication is a necessity to prepare a new set of photons before running each "shot" of the experiment. These issues are not present in the proposed BEC-trap platform.

1.2. Atomic boson sampling of massive interacting atoms in a BEC trap

Rather than using non-interacting photons, atomic boson sampling takes atom number measurements of subsets of excited states in an equilibrium BEC gas. This remarkably leads to the same ♯P-hard complexity that is present in the optical system, with a number of possible benefits. In particular, rather than having to load the system for each "shot" with prepared photonoic states, the atomic system "squeezes itself" once loaded requiring no sophisticated external sources of bosons in quantum states. Likewise it is possible that multiple measurements can be taken for the same system over a period of time rather than just one.

The complexity of atomic boson sampling comes from the combination of the squeezing and interference between bare-atom states due to their coupling into quasiparticles. Both phenomena occur naturally in the system due to interparticle interactions. It is paramount that both are present, as one without the other is not sufficient for the computational ♯P-hardness.

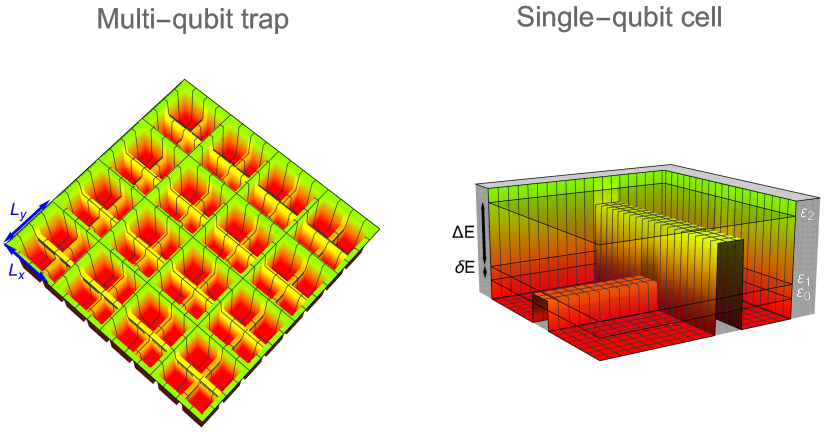

Figure 1. 2D model of a BEC trap made up of multiple single-qubit cells each of size $L_x \times L_y$. Each has at least two lower energy levels. They contribute to the lower-energy miniband separated from the higher energy levels by an energy gap ΔE larger than the lower-energy splitting δE.

1.3. Why multi-qubit trap? Necessary requirements for the BEC trap

To make atomic boson sampling nontrivial, the multi-qubit trap must be designed in such a way as to ensure spreading of the condensate across the entire trap while still allowing for Bogoliubov coupling to occur between a large number of bare-atom excited states. It is desirable that the excited states should belong to a miniband, a group of states, which are separated from further excited states by a sufficient energy gap ΔE. Simultaneously, there must be sufficient variability possible to ensure that a large array of quantum-statistically correlated occupations of bare-atom excited states, significantly squeezed and coupled into quasiparticles, can be observed. Otherwise, the hafnian could be degenerate (as in [11]) and computable in polynomial time by some approximation algorithm. So, it is imperative that the model is built with multiple possible avenues for customization, such as varying the trapping potential, temperature, interaction, etc.

It is thus nontrivial to determine how one would best go about designing such a system. In this paper, we discuss an example of such a trap, the multi-qubit BEC trap sketched in figure 1, and its basic model. First, we explore the single-particle energy spectra and eigenstates. Then, the many-body properties are described numerically by solving the Gross-Pitaevskii equation for the condensate wave function and finding the Bogoliubov couplings required for estimates of the multimode squeezing parameters via Bogoliubov transformation diagonalizing Hamiltonian.

2. A model for the BEC trapping potential

The model we will use for the multi-qubit BEC trap is one of many adjacent single-qubit potentials in the form of rectangular cells with a single delta-function potential near its center. We consider either one- or two-dimensional (1D or 2D) configurations of the single-qubit cells. The reason we choose this system is because of its simplicity while still representative and providing a number of parameters which can be tuned to achieve a wide variety of outcomes.

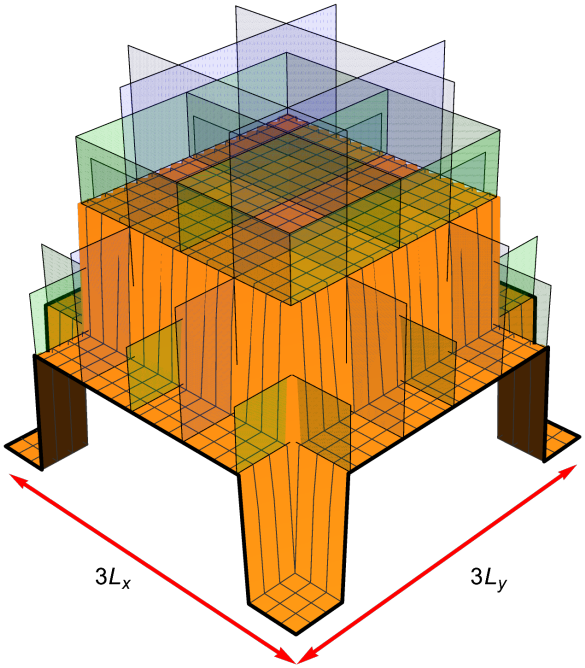

Figure 2. An example of a 2D multi-qubit BEC trap containing 3×3 single-qubit cells and a pedestal background potential (shown in yellow) as per the model in Eq. (2). The inter- and intra-cell delta-function potentials are shown by the purple and green semi-transparent sheets, respectively. For clarity, the infinitely high outer walls of the trap are not shown. The dimensions are $3L_x \times 3L_y$.

Let us enumerate the structure of a 1D trap. The base is an array of Q adjacent cells, each of which contains a single intra-cell delta potential at a location x_q. These cells are separated themselves by another, inter-cell delta potential at location X_q which can be independently controlled. The magnitudes of these potentials are given by ρ'_q and ρ_q, respectively. Each cell also has background flat potentials, with their magnitudes given by U_{2q-1} and U_{2q} for either side of the intra-cell delta potential. This in total leads to the following trapping potential

$$\begin{aligned} U(x) &= \sum_{q=1}^{Q} [\tilde{U}_{2q-1}(x) + \tilde{U}_{2q}(x) + \rho'_q \delta(x - x_q) + \rho_q \delta(x - X_q)] \quad \text{if} \quad x \in (0, QL); \\ U(x) &= \infty \quad \text{if} \quad x \leq 0 \quad \text{or} \quad x \geq QL, \end{aligned} \tag{1}$$

where $\tilde{U}_{2q-1} = U_{2q-1}[\theta(x - X_{q-1}) - \theta(x - x_q)]$ and $\tilde{U}_{2q} = U_{2q}[\theta(x - x_q) - \theta(x - X_q)]$, with $\delta(x)$ representing the Dirac delta function and $\theta(x)$ the unit step function. We ensure here that the choices of x_q and X_q are such that $0 = X_0 \leq x_1 \leq X_1 \leq x_2 \leq \cdots \leq X_{Q-1} \leq x_Q \leq X_Q = QL$. Note how the borders of the trap are fixed such that the total length is QL, but there is freedom to choose the exact location of each delta potential in the cell. Likewise the sets of parameters ρ_q, ρ'_q, U_{2q-1}, and U_{2q} could also be changed independently.

This model can be easily expanded for a 2D trap such as that seen in figure 2. Consider a 2D array of $Q_x \times Q_y$ cells. The potential can now be decomposed into separate x and y components

such that $U(x,y) = U^{(x)}(x) + U^{(y)}(y)$. Each component has a form similar to the 1D form in Eq. (1),

$$\begin{aligned} U^{(x)}(x) &= \sum_{q=1}^{Q_x} [\tilde{U}_{2q-1}^{(x)} + \tilde{U}_{2q}^{(x)} + \rho_q^{(x)\prime}\delta(x - x_q) + \rho_q^{(x)}\delta(x - X_q)] \quad \text{if} \quad x \in (0, Q_x L_x), \\ U^{(x)}(x) &= \infty \quad \text{if} \quad x \le 0 \quad \text{or} \quad x \ge Q_x L_x; \\ U^{(y)}(y) &= \sum_{q=1}^{Q_y} [\tilde{U}_{2q-1}^{(y)} + \tilde{U}_{2q}^{(y)} + \rho_q^{(y)\prime}\delta(y - y_q) + \rho_q^{(y)}\delta(y - Y_q)] \quad \text{if} \quad y \in (0, Q_y L_y), \\ U^{(y)}(y) &= \infty \quad \text{if} \quad y \le 0 \quad \text{or} \quad y \ge Q_y L_y. \end{aligned} \tag{2}$$

Potentials $\tilde{U}_j^{(x)}, \tilde{U}_j^{(y)}$ are defined analogous to that in Eq. (1). For simplicity's sake, we consider only symmetric traps: $L_x = L_y = L, \rho_q^{(x)} = \rho_j^{(y)} = \rho_q, \rho_q^{(x)\prime} = \rho_j^{(y)\prime} = \rho_q', \tilde{U}_j^{(x)} = \tilde{U}_j^{(y)} = \tilde{U}_j \ \forall q, j$.

3. Energy spectrum and solutions to the single-particle Shrödinger equation

3.1. One-dimensional multi-qubit trap

We present the results derived from the eigen-energy solutions to the 1D Schrödinger equation

$$\left(-\frac{\hbar^2}{2m}\frac{d^2}{d^2x} + U(x)\right)\psi_n(x) = \varepsilon_n\psi_n(x), \qquad n = 0, 1, 2\ldots, \tag{3}$$

by means of numerical plots, although analytical solutions for the model (1) also can be found.

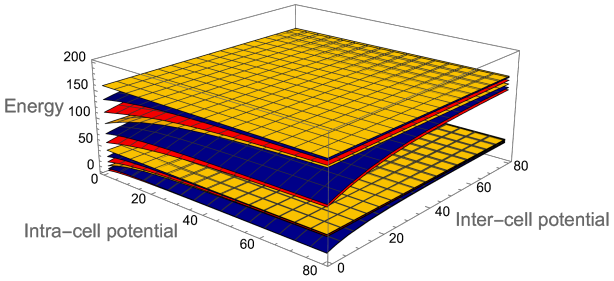

Figure 3. The first 12 single-particle energy levels for a 1D 3-qubit trap with zero background potential as they depend on the inter- and intra-cell potential strengths $\bar{\rho}_1 = \bar{\rho}_2$ and $\bar{\rho}_1' = \bar{\rho}_2' = \bar{\rho}_3'$.

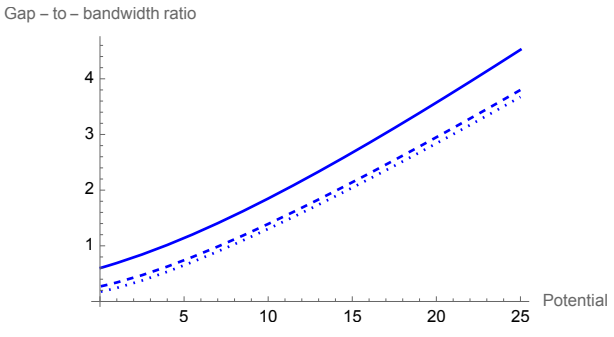

Figure 4. The ratio of the energy gap to the miniband width for the symmetric two- (solid), four- (dashed), and six- (dotted) qubit traps as a function of the equal dimensionless delta potentials $\bar{\rho}_1 = \bar{\rho}_2 = \bar{\rho}_1' = \bar{\rho}_2' = \bar{\rho}_3'$.

It is convenient to introduce dimensionless quantities for various parameters of the system, such as the background potential U_j, energy ε_n, and delta potential strengths ρ_q, ρ_q', as follows

$$\bar{U}_j = \frac{2mL^2}{\hbar^2}U_j, \qquad \bar{\varepsilon}_n = \frac{2mL^2}{\hbar^2}\varepsilon_n, \qquad \bar{\rho}_q = \frac{2mL}{\hbar^2}\rho_q, \qquad \bar{\rho}_q' = \frac{2mL}{\hbar^2}\rho_q'. \tag{4}$$

In all cases, the value of L is taken to be the length of a single-qubit cell in the overall trap.

As a representative example, consider a chain of $Q = 3$ single-qubit cells. The energy spectrum for such a trap is shown in figure 3 for various values of the inter- and intra-cell potentials. Note how for very low potential barriers, the spectrum is just that of the uniform box trap, with quadratic spacing between each level. As the delta potentials are increased, the expected mini-band structure emerges, where there is a tight grouping of the first $2Q = 6$ levels, a large gap in energy before the next, seventh level and a tight grouping of the second 6 levels.

The figure of merit here is the ratio of the width of the first energy miniband to the gap between the first two energy minibands. This is plotted in figure 4 for different delta-potential magnitudes. Note how in all cases higher potential barriers lead to a stronger separation of the minibands. However, one must be conscious of the fact that should the barriers become too high that an even spreading of the condensate will be impossible. Thus, a balance must be struck between a large energy gap and low enough barriers.

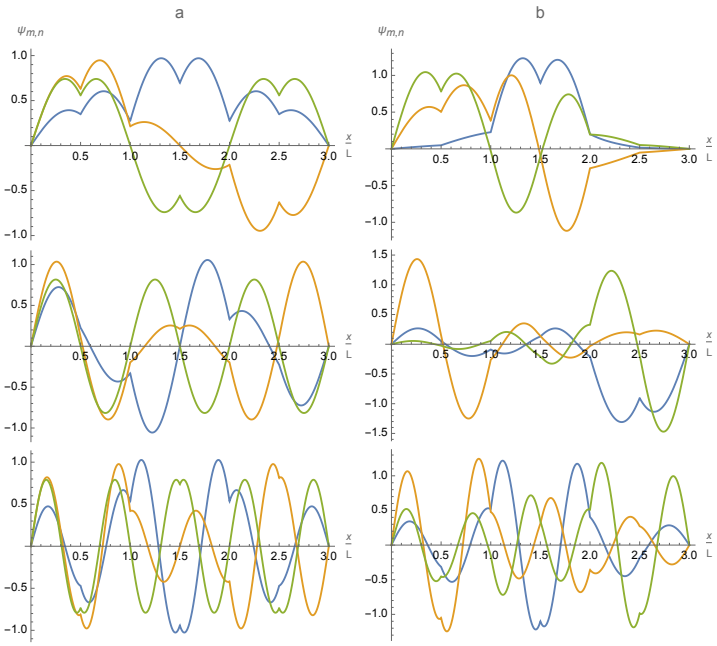

Figure 5. The first 3 subminibands of the eigenfunctions $\psi_{m,n}$ for the 1D 3-qubit trap. The first row is the lowest subminiband $m = 0$, followed by the next ones $m = 1$ and $m = 2$. In blue is $q = 1$, yellow is $q = 2$, and green is $q = 3$. In both figures a and b the delta potential strengths are $\bar{\rho}_1 = \bar{\rho}_2 = 22$ and $\bar{\rho}'_1 = \bar{\rho}'_2 = \bar{\rho}'_3 = 8$, though in figure a there is no background potential and in figure b the background potentials in each cell are $\bar{U}_j = 15, 0, 30$, respectively.

In order to see how the flat background potentials $\tilde{U}_j$ affect the system, it is enlightening to look at the eigenfunctions themselves rather than just the energy levels. The eigenfunctions are shown in figure 5. We enumerate each eigenfunction $\psi_{m,q}(x)$ with two integers labeling its eigen energy in increasing order. One for which subminiband it is a part of as $m = 0, 1, ...$ and one for the order of the eigen energy within that subminiband $q = 1, 2, ..., Q$. Note how the introduction of a background potential in some area serves to in general exclude the eigenfunction from this area. This is a useful tool to have access to in order to tune the shape of the eigenfunctions, in particular, to ensure an even spreading of the condensate.

The main effect of the delta function potentials on the eigenfunction comes in two flavors. Firstly, if the unperturbed eigenfunction has less natural zeros than the number of delta potentials, some of the delta functions will "dig down" into the eigenfunction trying to create new zeros under the delta-function potentials. However, sometimes if there is an existing zero nearby, instead of digging a new hole, the delta potential will simply drag an existing zero underneath it. Both of these effects can be observed in figure 5.

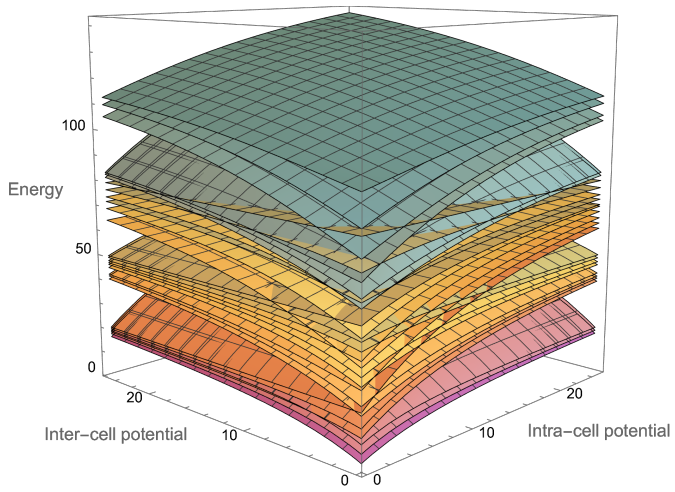

Figure 6. The first 48 energy levels for the single-particle states of a 2D (3×3)-qubit trap with zero background potential as they depend on the inter-cell and intra-cell delta potential strengths ($\bar{\rho}_1 = \bar{\rho}_2$ and $\bar{\rho}'_1 = \bar{\rho}'_2 = \bar{\rho}'_3$).

3.2. Two-dimensional multi-qubit trap

Expanding this model for the multi-qubit trap to two dimensions is quite easy: The seperable potential (2) leads to seperable solutions for the 2D Schrödinger equation. Thus, analysis of the energy levels and eigenfunctions can be done in a similar fashion to the 1D case.

To get the energy spectrum of the 2D system all additive combinations of the existing energy levels for each of two 1D traps have to be taken. This leads to an interesting situation where different combinations of energy levels may "cross" each other as you explore different values of the delta-function potentials, as can be seen in figure 6. The effect of the flat background potentials $\tilde{U}_j$ on the ground-state eigenfunction $\psi_0(x, y)$ in two dimensions is shown in figure 7.

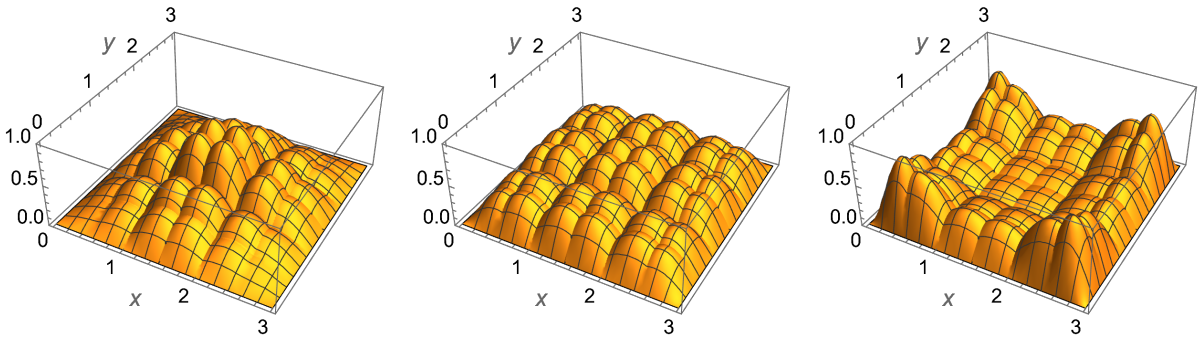

Figure 7. The ground-state eigenfunction $\psi_0(x, y)$ for the (3×3)-qubit trap with $x-y$ symmetric 1D inter- and intra-cell delta potentials $\bar{\rho}_1 = \bar{\rho}_2 = 4$ and $\bar{\rho}'_1 = \bar{\rho}'_2 = \bar{\rho}'_3 = 8$, respectively, for the case of a central pedestal of a flat background potential with the strength $\bar{U}_j = 0$ (Left), 6 (Center), 12 (Right) localized within the central square $|x - 3L/2| < L$ & $|y - 3L/2| < L$.

4. Condensate wave function versus single-particle ground state

The next logical exploration in this design is to see how the ground state is affected by the interpatricle interactions through solving the Gross-Pitaevskii equation for the condensate

$$\left(-\frac{\hbar^2\Delta}{2m} + U(\mathbf{r}) + gN_0|\phi_0(\mathbf{r})|^2 + 2gn_{ex}(\mathbf{r}) - \mu \right)\phi_0 = 0, \quad g = \frac{4\pi\hbar^2 a}{m}. \tag{5}$$

(We use standard notations [3].) The strength g of interaction depends on the healing length

$$\xi = \hbar/\sqrt{2mgN/V} = 1/\sqrt{8\pi aN/V} \ . \tag{6}$$

As the interpatricle interactions increase, the condensate begins to more evenly spread itself throughout the trap. When $\xi \gg L$ the gas acts almost as an ideal gas. The reverse is also true, where a small healing length relative to the trap size will mean that the interaction between atoms to become significant. This works in opposition to the trap itself which is created to partition the condensate into separate cells. The effect of interaction is shown in figures 8, 9.

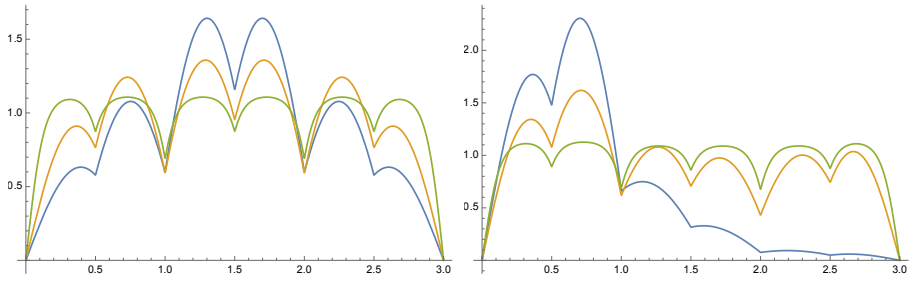

Figure 8. The ground state wavefunction for the 1D 3-qubit trap with zero (blue), moderate ($L/\xi = 2$, yellow) and strong ($L/\xi = 10$, green) interaction. The left graph is for a symmetric trap with no background potential while the right is for an asymmetric trap with background potentials $\bar{U}_j = 8$ for $1 < x/L < 2.5$. In all cases $\bar{\rho}_1 = \bar{\rho}_2 = 16$, $\bar{\rho}'_1 = \bar{\rho}'_2 = \bar{\rho}'_3 = 8$.

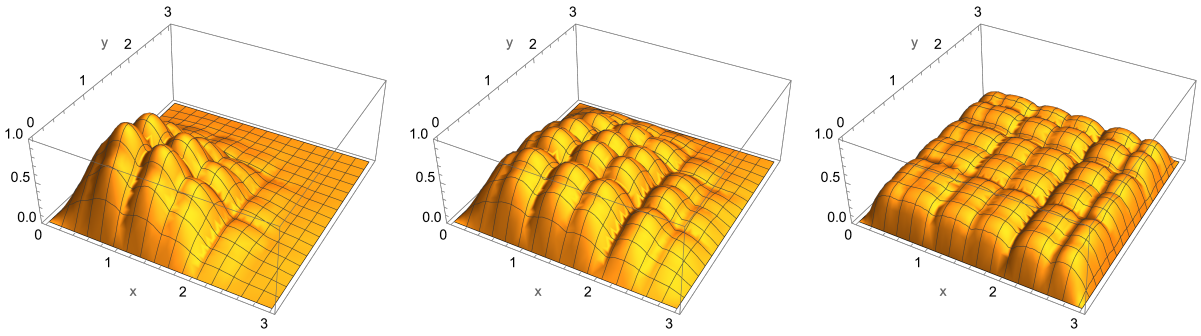

Figure 9. The ground state wavefunction for the 2D (3×3)-qubit trap with zero background potential and zero (left), moderate ($L/\xi = 5$, middle) and strong ($L/\xi = 20$, right) interaction. 1D $x-y$ symmetric inter- and intra-cell delta potentials are $\bar{\rho}_2 = 2\bar{\rho}_1 = 10$, $\bar{\rho}_3{}' = 2\bar{\rho}_2{}' = 4\bar{\rho}_1{}' = 8$.

Firstly, it can be seen that with increasing interaction, the regions near the inter- and intra-cell delta potentials where the wavefunction is suppressed tend to shrink. The repulsion experienced by the atoms pushes them into the previously unoccupied region. This is favorable for the appearance of the ♯P-hardness of boson-sampling computing as it increases the number of coupled bare-atom excited states in the system. This is also useful as it provides yet another metric outside of the background potential that can be used to "shape" the condensate.

Also of note in these solutions to the Gross-Pitaevskii equation is how asymmetric traps are affected. Increasing the interparticle interaction tends to homogenise the condensate not only in terms of its overall occupation, but also its shape. As seen in figure 8, although the two traps have different background step potentials, one symmetric and one asymmetric, both begin to look nearly identical for the sufficiently strong interparticle interaction, i.e., large ratio $L/\xi \gg 1$.

5. Bogoliubov couplings and quasiparticles – causes for squeezing and interference
Statistics of atomic boson sampling and its computational ♯P-hardness are determined by a covariance matrix G which is expressed via the matrix R of the Bogoliubov transformation [3]:

$$G \equiv \left\langle : \begin{pmatrix} \hat{\mathbf{a}}^\dagger \\ \hat{\mathbf{a}} \end{pmatrix} \begin{pmatrix} \hat{\mathbf{a}}^\dagger \\ \hat{\mathbf{a}} \end{pmatrix}^T : \right\rangle = R\mathbb{D}R^\dagger + \frac{RR^\dagger - \mathbb{1}}{2}; \;\; \mathbb{D} = \begin{bmatrix} D & 0 \\ 0 & D \end{bmatrix}, \quad D = \bigoplus_j \frac{1}{e^{E_j/T} - 1}. \tag{7}$$

Here E_j is an energy of the j-th quasiparticle. The matrix R performs the transformation

$$\begin{pmatrix} \hat{\mathbf{a}}^\dagger \\ \hat{\mathbf{a}} \end{pmatrix} = R \begin{pmatrix} \hat{\mathbf{b}}^\dagger \\ \hat{\mathbf{b}} \end{pmatrix}, \qquad R = \begin{bmatrix} U^* & 0 \\ 0 & U \end{bmatrix} \begin{bmatrix} \cosh r & (e^{i\theta} \sinh r)^* \\ e^{i\theta} \sinh r & \cosh r^* \end{bmatrix}, \tag{8}$$

from quasiparticle creation and annihilation operators $\hat{\mathbf{b}}^\dagger = (\hat{b}_1^\dagger, \hat{b}_2^\dagger, \ldots)^T$ and $\hat{\mathbf{b}} = (\hat{b}_1, \hat{b}_2, \ldots)^T$ to bare-particle operators $\hat{\mathbf{a}}^\dagger$ and $\hat{\mathbf{a}}$ in the representation of the excited-particle field operator

$$\hat{\psi}_{\rm ex}(\mathbf{r}) = \sum_{k \neq 0} \phi_k(\mathbf{r}) \hat{a}_k = \sum_j \left(u_j(\mathbf{r}) \hat{b}_j + v_j^*(\mathbf{r}) \hat{b}_j^\dagger \right). \tag{9}$$

The matrix R is determined by the condensate wavefunction and Bogoliubov couplings [3]

$$\Delta_{kk'} = gN_0 \int \phi_k^*(\mathbf{r}) \, |\phi_0(\mathbf{r})|^2 \, \phi_{k'}(\mathbf{r}) \, d^3\mathbf{r}, \quad \tilde{\Delta}_{kk'} = gN_0 \int \phi_k^*(\mathbf{r}) \, \phi_0(\mathbf{r})^2 \, \phi_{k'}^*(\mathbf{r}) \, d^3\mathbf{r}. \tag{10}$$

Here excited states ϕ_k are orthogonal to the condensate wavefunction ϕ_0. They can be obtained

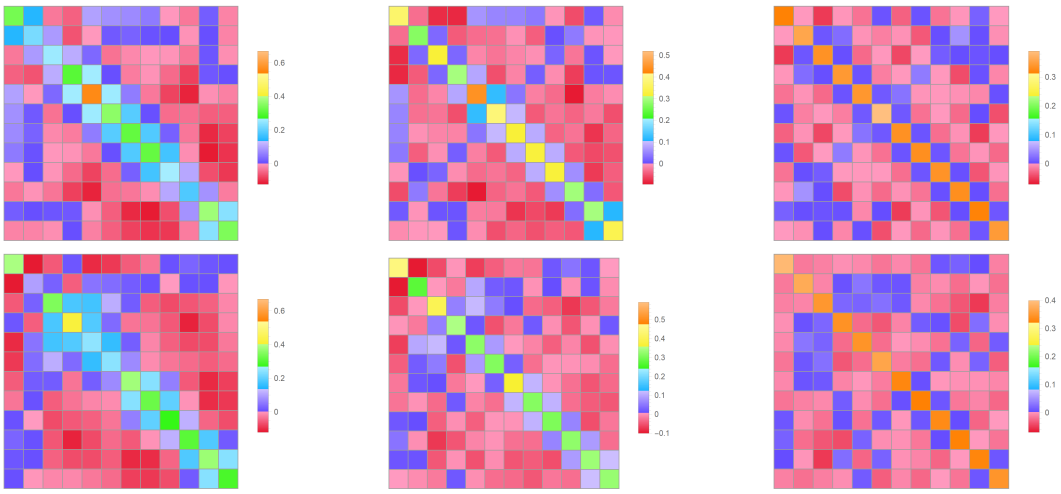

Figure 10. Matrix of Bogoliubov couplings (10) between the first 12 excited states for the asymmetric 1D 3-qubit trap shown in figure 8. Excited states are set by the Gram–Schmidt orthogonalization from the condensate ϕ_0 and (upper row) the sine functions $\sin(k\pi x/(4L)), k = 1, \ldots, 12$, or (lower row) the first 12 eigenfunctions of the single-particle Schrödinger equation (3) in the case of zero (left), moderate ($\frac{L}{\xi} = 2$, middle), and strong, ($\frac{L}{\xi} = 10$, right) interaction.

by means of the Gram–Schmidt orthogonalization from the condensate wavefunction ϕ_0 and any basis in the single-particle Hilbert space. Typical couplings are shown in figure 10.

It clearly illustrates very interesting, nontrivial patterns in the distribution of couplings. Due to the traps asymmetry, the essentially non-zero Bogoliubov couplings extend outwards past the

main diagonal even in the case of a weak interaction, $L/\xi \ll 1$. When the interaction becomes strong, $L/\xi \gg 1$, and suppresses the asymmetry, the main diagonal becomes uniformly occupied by anomalously large couplings and simultaneously a checker-board pattern appears along with an anti-diagonal of almost zero couplings. The maximum spread and mess in the distribution of couplings arises in the case of a moderate interaction, $L/\xi \sim 1$, that supports the idea of a moderate interaction being optimal for the computational ♯P-hardness of boson sampling.

Another important fact is that changing the detectors' basis from the sine functions to those of single-particle eigenfunctions has a large impact on the structure of couplings. Though some of the major features remain, the nuances of the essentially non-zero entries changes drastically.

The overall takeaway of this is that the proposed multi-qubit structure for the BEC trap provides sufficient complexity and variability to ensure a wide variety of matrix hafninans is envolved, potentially leading to the computational ♯P-hardness of atomic boson sampling.

6. Conclusions

We described the properties of a multi-qubit BEC trap for the purpose of atomic boson sampling which manifests ♯P-hard complexity. In particular, we elaborated on the single-particle eigen functions and energies using the Schrödinger equation and on the effects of the interparticle interaction through the condensate wavefunction, described by the Gross-Pitaevskii equation, and Bogoluibov couplings. Throughout both 1D and 2D multi-qubit BEC traps were considered for both symmetric and asymmetric trapping potentials.

The multi-qubit BEC trap as described above offers a robust platform for atomic-boson-sampling experiments. Creation of such a system looks feasible in view of recent advances in the BEC trapping, cooling and detecting technologies. Compared to the experiments on fluctuations of the total noncondensate occupation [12, 13], one should just additionally split the noncondensate into many parts associated with different groups of excited states and measure their occupation numbers. Although initial experiments will be limited in scope, it is likely with enough effort quantum supremacy could be demonstrated.

Acknowledgements

W.S. acknowledges the support from the Herman F. Heep and Minnie Belle Heep Texas A&M University Endowed Fund via a fellowship in the Institute for Quantum Science and Engineering.

References

[1] Harrow, A.W.; Montanaro, A. Quantum computational supremacy. *Nature* **2017**, *549*, 203.
[2] Tarasov, S.; Shannon, W.; Kocharovsky, V.V.; Kocharovsky, Vl.V. Multi-qubit Bose-Einstein condensate trap for atomic boson sampling. *Entropy* **2022**, *24*, 1771.
[3] Kocharovsky, V.V.; Kocharovsky, Vl.V.; Tarasov, S.V. Atomic boson sampling in a Bose-Einstein-condensed gas. *Phys. Rev. A* **2022**, *106*, 063312.
[4] Aaronson, S.; Arkhipov, A. The computational complexity of linear optics. *Theory Comp.* **2013**, *9*, 143–252.
[5] Lund, A.P. *et al.* Boson Sampling from a Gaussian State, *Phys. Rev. Lett.* **2014**, *113*, 100502.
[6] Wang, H. *et al.* High-efficiency multiphoton boson sampling. *Nature Photonics* **2017**, *11*, 361–365.
[7] Zhong, H.-S. *et al.* Quantum computational advantage using photons. *Science (N.Y.)* **2020**, *370*, 1460–1463.
[8] Kocharovsky, V.V.; Kocharovsky, Vl.V.; Tarasov, S.V. The Hafnian Master Theorem. *Lin. Algebra Appl.* **2022**, *651*, 144–161.
[9] Kocharovsky, V.V.; Kocharovsky, Vl.V.; Tarasov, S.V. Unification of the Nature's Complexities via a Matrix Permanent – Critical Phenomena, Fractals, Quantum Computing, ♯P-Complexity. *Entropy* **2020**, *22*, 322.
[10] Valiant, L.G. The complexity of computing the permanent. *Theor. Comput. Sci.* **1979**, *8*, 189–201.
[11] Kocharovsky, V.V.; Kocharovsky, Vl.V.; Martyanov, V.Yu.; Tarasov, S.V. Exact recursive calculation of circulant permanents: A band of different diagonals inside a uniform matrix. Entropy **2021**, *23*, 1423.
[12] Tarasov, S.V.; Kocharovsky, Vl.V.; Kocharovsky, V.V. Bose-Einstein-condensate fluctuations versus an interparticle interaction. *Phys. Rev. A* **2020**, *102*, 043315.
[13] Kristensen, M.; Christensen, M.; Gajdacz, M. *et al.* Observation of atom number fluctuations in a BEC. *Phys. Rev. Lett.* **2019**, *122*, 163601.